Proceedings of the 48th National Conference on Fluid Mechanics and Fluid Power (FMFP)
December 27-29, 2021, BITS Pilani, Pilani Campus, RJ, India
FMFP2021–04–175

Large Eddy Simulation of a confined planar jet opening in a rectangular channel

Binayak Lohani[1], Ashley Melvin[2], Manaswita Bose[3]

[1]Department of Mechanical and Aerospace Engineering, IOE Pulchowk Campus, Lalitpur, Nepal
[2]FOSSEE, IIT Bombay, Mumbai, 400076, India
[3]Department of Energy Science and Engineering, IIT Bombay, Mumbai 400076, India

ABSTRACT

The primary aim of the present work is to simulate the laminar-turbulent transition of confined planar jet opening in a rectangular channel using Large Eddy Simulation (LES), as implemented in OpenFOAM. The sub grid scale turbulence was captured by the Smagorinsky model with Van Driest damping function. Simulations were performed on resolved grids and for different Reynold numbers. Q-criterion and the components of the Reynolds stress tensor were determined after the simulations were initially stabilized. Mean velocity profile at the midplane of the channel was compared with the analytical result of the damped flow. Strength of the entrained vortex was determined. Pressure fluctuations at the jet inlet were analysed. Transition was observed at channel-based Reynolds number of lower than 1200.

Keywords: CFD, OpenFOAM, LES, planar jet, transition.

1. INTRODUCTION

Turbulent flow in a rectangular channel is a classical problem in Computational Fluid Dynamics (CFD) for investigating the turbulent characteristics in the flow. With the involvement of jet at the inlet of the channel makes the present work a combination of two widely conducted LES studies lately. Turbulent flows consist of eddies with a range of sizes and energies. The most commonly used turbulence modelling technique is RANS (Reynolds Averaged Navier Stokes) where every eddy in the flow is modelled. On the other hand, in DNS (Direct Numerical Simulation), all the eddies are resolved; however, this method is computationally intensive. In LES, the large eddies in the flow are resolved whereas smaller eddies are modelled as in the RANS approach. The LES method strikes a balance between the requirement in the computational resources and the temporal and spatial resolutions in the flow description. The aim of the present work is to simulate the behaviour of a confined planar jet using LES on OpenFoam platform.

2. LITERATURE REVIEW AND OBJECTIVE

The flow structures vary significantly even at low Reynolds number in a jet flow condition [1]. Practically, the jet flow consists of eddies that may be tiny or large irrespective of the Reynolds number. Two low-Reynolds number cases were studied in a free circular jet flow and the observed transition occurred for Reynolds number in the range $680 - 1030$ [2].

A number of experimental and computational studies have investigated the behaviour of turbulent eddies in the channel [3]. Most of the previous work focused on the instabilities occurring in the circular jet. Imparting perturbations at inlet conditions assisted for the onset of instabilities and critical Reynolds number was found at the range of $500 - 525$. Without the perturbation the critical Reynolds number was observed at the range of $900 - 925$ which was analysed using Direct Numerical Simulation (DNS)[4, 5]. A study on statistical transition to turbulence on plane channel flow conducted by the authors estimated the critical point at Re$\simeq$965 [6]. Aspect ratio of the rectangular channel also plays an important role in the laminar-turbulent transition in the flow. A linear stability analysis concluded that critical Reynolds number may vary with the aspect ratio of the channel. For an aspect ratio of 3.92, the critical Reynolds number is found to be 2315. According to the trend observed by the authors, critical Reynolds number increases for the channel with higher aspect ratio [7, 8].

The objective of the present work is to investigate the transition behaviour of the flow of a planar jet opening in a confined channel. To that end simulations were carried out for several cases with Reynolds number ranging between 100 and 2400. Fluid phase turbulence was modelled following the principles of Large Eddy Simulations (LES) as implemented on the opensource software OpenFOAM. Simulations were carried out for a wide range of Reynolds numbers. Dependence of grid resolution with changing Reynolds number was analysed carefully. The velocity fluctuations, power spectrum of velocity and pressure, evolution of the RMS velocity profiles, the Reynolds stress terms, and "Q" criterion were determined. The methodology followed in the present work is discussed in the next section.

3. MATERIALS AND METHODS

A rectangular channel of aspect ratio, $A = 0.25$ (defined by equation 1) and air as working fluid was used in the computational analysis of the confined planar jet flow. The height of the channel is twice of the jet height at the inlet. The length of the channel was carefully chosen for the fully developed flow in laminar as well as turbulent regime. According to the conclusions drawn in [9], the length of the channel for a fully developed turbulent flow should be at least 130 times the height of the channel. So, the length of the channel for the simulation is maintained at $1.5\ m$.

S. Bhattacharyya and A. C. Benim (eds.), *Fluid Mechanics and Fluid Power (Vol. 2)*,
Lecture Notes in Mechanical Engineering, https://doi.org/10.1007/978-981-19-6970-6_67

$$A = \frac{W}{S} \quad (1)$$

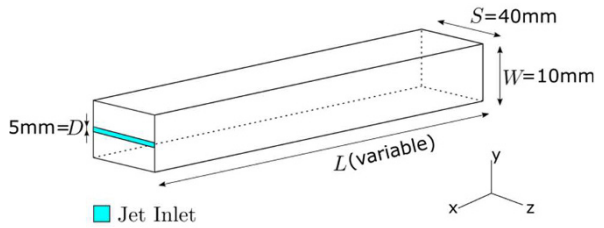

Figure 1: Schematic diagram of the channel

For an unsteady, incompressible flow, mass and momentum conservation equations, in the absence of any external forces, can be expressed as in equation (2) and (3) respectively. These equations were solved in the grid using the "Pimple Algorithm".

$$\nabla . \mathrm{u} = 0 \quad (2)$$

$$\frac{\partial \mathrm{u}}{\partial t} + \nabla . (\mathrm{u} \otimes \mathrm{u}) = -\frac{1}{\rho}\nabla \mathrm{P} + \nu \nabla^2 u \quad (3)$$

The instantaneous velocity term can be represented as a sum of fluctuating and mean velocity as in equation (4). The mean velocity can be modelled using RANS simulation but it does not predict the fluctuating part of velocity. So, to capture the fluctuating part, LES is selected.

$$u = u' + u_m \quad (4)$$

LES resolves only those eddies which are larger than the length scale Δ. However, eddy which is smaller than the given length scale in the flow is modelled using the sub grid turbulence model. Smagorinsky model developed in 1963 which assumes the sub grid eddies present in the viscous sublayer is attributed for simulation. In order to have the perfect resolution to capture the turbulence in the flow, proper discretization of the domain is necessary. The smallest grid in the domain should be in the order of Kolmogorov's length scale (η). This scale resembles the smallest eddies present in the flow which is a function of Re (equation 5). This scaling is usually assumed to resolve the turbulent eddies in the flow and is generally used for DNS class of simulation near the wall regions.

$$\frac{\eta}{W} = Re^{-\frac{3}{4}} \quad (5)$$

For simulations following LES algorithms, the grid size needs to resolve the larger eddies and model the tiny eddies present in the flow. Hence, the length scale larger than η is employed for such calculations. However, the scaling should not exceed 10η to obtain results with better accuracy in LES. The time step is to be considered in a way so that it captures the required turbulent phenomenon in the domain. So, the Courant-Fell Lewi (CFL) number, expressed in equation (6), is the important parameter to be considered for such simulations. Lower the CFL number, higher the accuracy of the simulation to capture turbulent structures.

$$CFL = \frac{u_m \Delta t}{\Delta x} \quad (6)$$

Since the flow is bounded by walls on all four directions being a confined case, the first cell height of the grid was chosen so that the resolution of 4η criteria is fulfilled for every Re cases whose dimension is equivalent to that using $\Delta^+ = 2.2$ in each direction. The mesh was generated through blockMesh with simple grading using expansion ratio for a non-uniform mesh stretched near the walls of the channel and inlet of the jet. Details of mesh configuration used in the present study are shown in table 1.

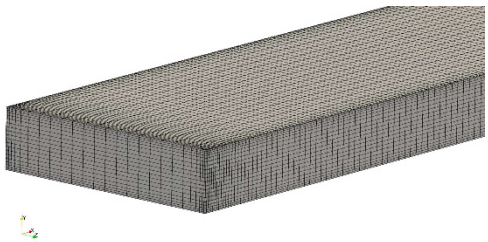

Figure 2: Mesh diagram of the computational domain for $Re = 2400$

The significance of imparting perturbation even at a low-Reynolds number jet inlet case was discussed in [1]. Giraldo et al. conducted a detailed study of the inlet condition of the jet to produce more coherent turbulent structures and adequate velocities [10]. They have noted that the fluctuating boundary condition available in OpenFOAM over-estimates the velocity decay although giving acceptable results. Realistic inflow condition is necessary because it may affect the downstream turbulent characteristics [11]. Therefore, the "turbulentInlet" boundary condition of OpenFOAM was attributed at the inlet of the jet which yields the spatio-temporal variant field by summing a set of pseudo-random numbers.

Table 1: Details of Mesh Configuration for confined geometry

Re	$N_x \times N_y \times N_z$	Δ (in m)	Δt (s)
100	$220 \times 11 \times 16$	$1.26e-03$	$1.5e-03$
1200	$566 \times 20 \times 26$	$1.96e-04$	$6.5e-05$
1800	$630 \times 26 \times 30$	$1.44e-04$	$3.6e-05$
2400	$670 \times 28 \times 40$	$1.16e-04$	$2.8e-05$

4. RESULTS AND DISCUSSION

Simulations were carried out for a wide range of Reynolds numbers starting from $Re = 100$; however, results for only four cases are discussed here. 24 cores were employed to perform the simulation.

4.1 Velocity Signal and Power Spectrum

The instantaneous velocity components of the fluid were recorded at a frequency of $15kHz$. Figure 3 shows the time evolution of the instantaneous velocity components for four different Reynolds numbers recorded at two different axial positions in the channel. In fig. (3a), fluctuations in the

streamwise velocity for $Re = 100$ was negligible even at $x = 0.5\ m$; however, for $Re = 1200, 1800$ and 2400, significant fluctuations were observed. Similar observations were made for the cross-gradient components of the velocities. It suggests that the disturbances at the inlet for the low Re, were already damped out at this position i.e., $(0.5, 0, 0)\ m$. On comparison of the fluctuation at two different locations of the channel in fig. [3(a, b & c)] and [3(d, e & f)], it was observed that the fluctuations in u, v and w components of velocity were much larger when the flow was closer to the jet. The fluctuation in the mean flow direction increases with the increasing Reynolds number or velocity of the jet.

To understand the turbulent flow from the jet, the power spectrum of the velocity signal near the jet inlet was studied. The spectrum was obtained and plotted on a logarithmic scale. The magnitude of the strength of the eddies, as it evolves or dissipates through time, can be deciphered from the power spectrum.

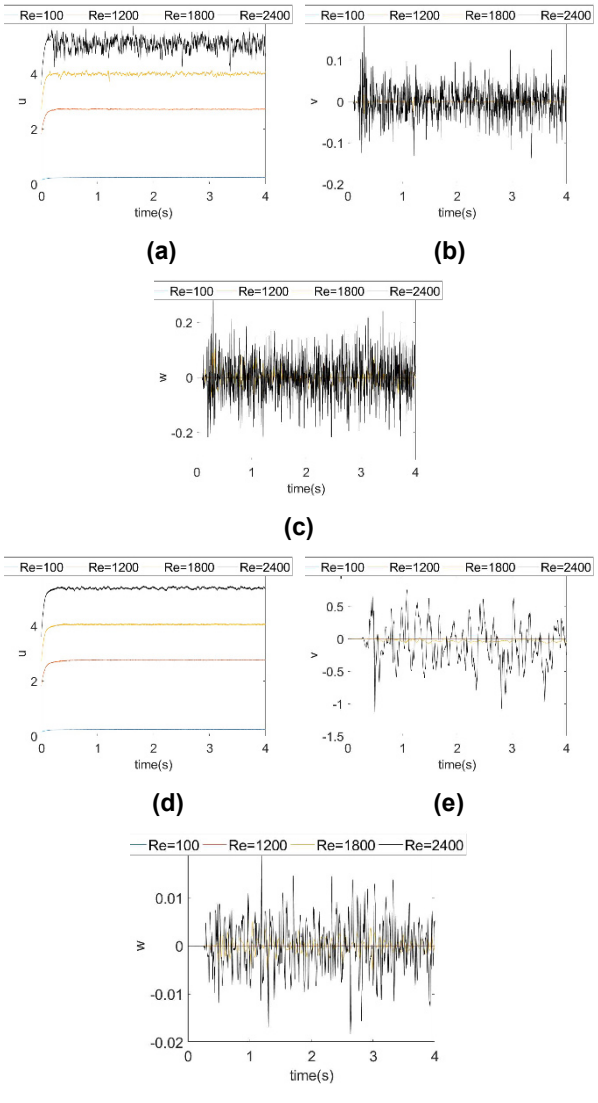

Figure 3: Components of instantaneous fluid velocities, [(a) & (d) u, (b) & (e) v, (c) & (f) w] determined at two different locations in the channel; (a) - (c) at $x = 0.5\ m$, (d)-(f) at $x = 1.4\ m$

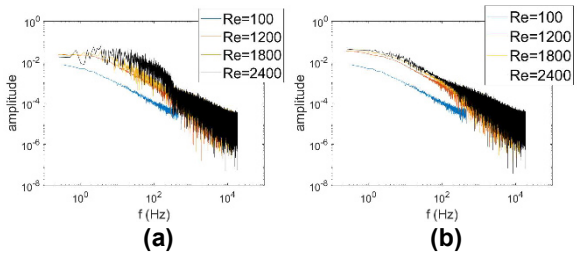

Figure 4: Power Spectrum of velocity signals (a) at $(0.5, 0, 0)m$, (b) at $(1.4, 0, 0)m$ for $Re = 100$, $1200, 1800$ and 2400

The power spectrum was plotted for each signal (Fig 4). The amplitude or strength of the vortices in the flow was increased for higher Reynolds number cases.

4.2 Spatial and Temporal Convergence

For a spatial convergence criterion, 3 different positions at $x = 1.38m, 1.4m$ and $1.42m$ when $t = 4s$ along the mean flow direction was taken. Meanwhile, to validate the temporal convergence, the velocity profile at 3 different time steps at $t = 3.8, 3.9$ and 4 seconds was plotted at 1.4m downstream of the flow direction. These convergence criteria aided to decide whether the flow was fully developed at a particular time in space. Higher Reynolds number case converges at longer mean flow dimension and time. Hence, convergence of $Re = 2400$ concludes the convergence of the flow with lower Re. It was observed that for $Re = 2400$ (Figs 5a and 5b) for a confined case, the convergence criteria were fulfilled. Convergence in spatial and temporal domain suggested the flow to be fully developed at the given location around $x = 1.4m$ and $t = 4s$.

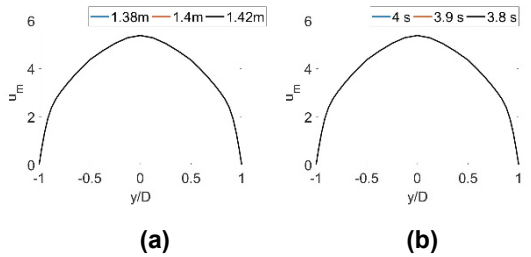

Figure 5: Mean Velocity Profiles of $Re = 2400$. (a) spatial and (b) time convergence

Next, the convergence of the root mean squared of the fluctuating velocity components was examined. The Reynolds stress terms in the principal diagonal of stress tensor are $< u'u' >, < v'v' >$ and $< w'w' >$. Square root of these quantities, normalized by the channel averaged velocity (u_m) was plotted in Fig 6.

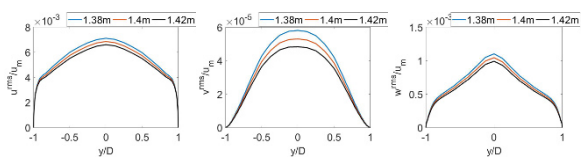

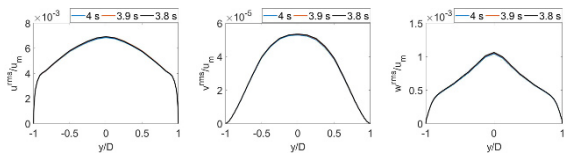

(a)

(b)

Figure 6: Profiles of fluctuating velocity of $Re = 2400$. (a) spatial and (b) temporal convergence

The off-diagonal elements of the Reynolds stress tensor, normalized by the square of the cross-section averaged mean velocity, were plotted against the wall normal direction. Fig. 7 shows the superposed profiles of the normalized off-diagonal elements plotted at different time instants at one axial position; and at three different axial positions at a given time. The mean behaviour of the components of the Reynolds stress tensor remains largely unchanged beyond $x = 1.4m$ and $t = 4s$.

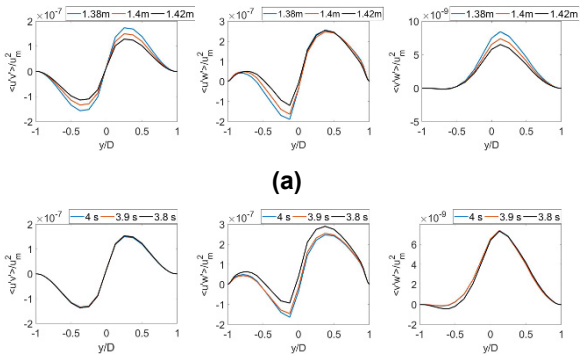

(a)

(b)

Figure 7: Profiles of turbulent shear stress of $Re = 2400$. (a) spatial and (b) temporal convergence

4.2.1 Comparison with the analytical profile

Next, the converged fully developed profile was compared with the analytical expression (equation 7) proposed by Theofilis et al. [8], for a fully developed laminar flow in a confined rectangular channel with aspect ratio A. U, Y_o and Z_o in equation (7) was normalized as shown in equation (8). W is the channel width.

$$U(Y_o, Z_o) = \left[(1 - Y_o^2) - \frac{32}{\pi^3}\sum_{n=0}^{\infty} \frac{(-1)^n \cosh\left\{\frac{(2n+1)\pi Z_o}{2}\right\}}{(2n+1)^3 \cosh\left\{\frac{(2n+1)\pi}{2A}\right\}} \times \cos\left\{\frac{(2n+1)\pi Y_o}{2}\right\}\right] \quad (7)$$

$$U = \frac{u}{u_{max}}, \qquad Y_o = \frac{2y}{W}, \qquad Z_o = \frac{2z}{W} \quad (8)$$

Figure 7 shows the velocity profiles plotted at various locations in the spanwise direction in the channel. The analytical expressions evaluated at corresponding Z_o were superposed on the graph. The plot showing velocity profiles for $Re = 100$ almost perfectly agrees with the analytical result.

Next, the profiles obtained for $Re = 1200, 1800$ and 2400 were compared against the analytical result. The simulated profiles agree closely with the analytical profile near the wall; however, closer to the centre of the channel, deviation between the simulated results and the analytical profile was observed. The simulated mean velocity profiles have a sharper near wall gradient as compared to the analytical results. The profile averaged values agreed closely between analytical and all the simulated Reynolds number. This indicates the similarity in the volumetric flow rate of the compared cases. However, the difference between the analytical profile and the simulated results indicates local vortical structures in the flow.

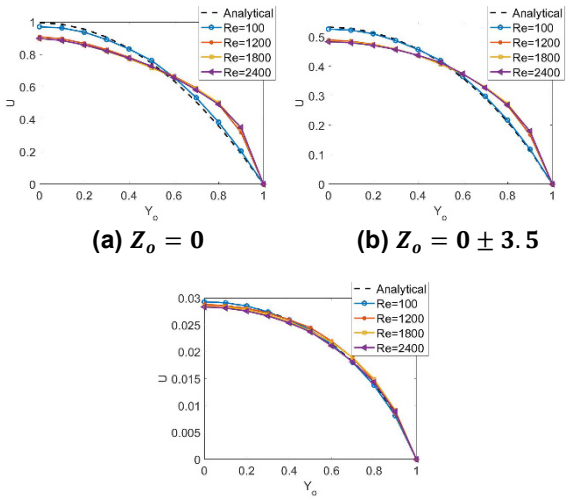

(a) $Z_o = 0$ **(b) $Z_o = 0 \pm 3.5$**

(c) $Z_o = 0 \pm 3.8$

Figure 8: Comparison of the analytical velocity profiles with simulation results at five different spanwise locations in the channel; solid lines represent the simulated profiles, dashed lines show the analytical solution

4.3 Vortical structures using Q-criteria

Q-criteria, a popular technique to visualize the coherent vortical structures in the flow, is based on the gradient of velocity of the flow. It is a magnitude of relative difference between vorticity (ω) and strain rate tensor (S). Figure 9, shows the turbulent eddies in the flow for all the cases in terms of the iso-surface of Q-criterion function. For $Re = 100$ *and* 1200, the turbulent eddies were damped out as soon within $0.1m$ downstream, while for $Re = 1800$ and 2400 the eddies generated by the jet was dissipated at around $0.3m$ and $0.6m$ respectively.

$$Q = \frac{1}{2}(trace(\omega)^2 - trace(S)^2) \quad (9)$$

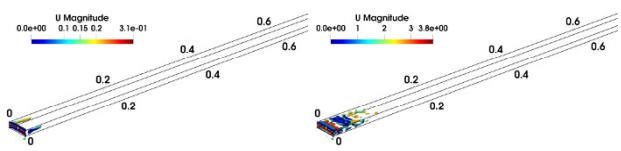

(a)$Re = 100$ **(b) $Re = 1200$**

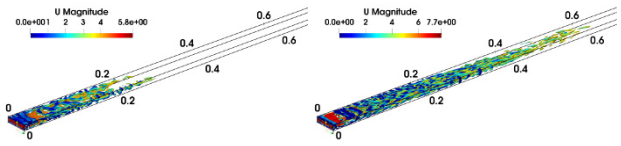

(b)$Re = 1800$ (d) $Re = 2400$

Figure 9: Isosurface of Q-criterion with value 500 at fully developed condition ($x = 1.4m$ and $t = 4s$)

The presence of corner eddies generated by the walls was represented using contours of Q-criteria at the flow - normal plane of the channel at fully developed condition (see Fig 10). Magnitude of "Q" increased as corresponding *Re* was increased indicating the presence of vortices in the flow.

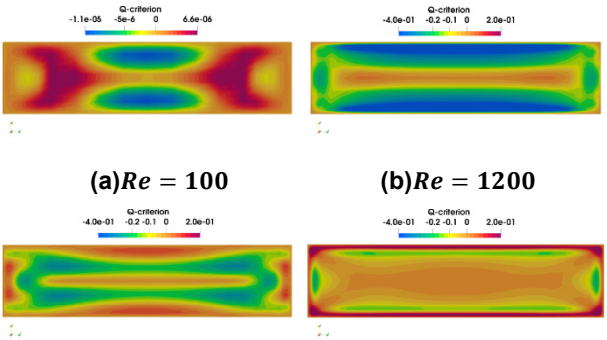

(a)$Re = 100$ (b)$Re = 1200$

(c)$Re = 1800$ (d)$Re = 2400$

Figure 10: Contours of Q-criteria at the flow-normal plane at fully developed condition ($x = 1.4m$ and $t = 4s$)

4.3.1 Analysis of vortex length and suction pressure

Vortices were generated near the inlet of the channel due to the pressure difference between the entering jet and the surrounding fluid in the channel.

The streamlines of the jet at the inlet for all Reynolds number cases at $t = 4s$ was shown in fig. (10). The vortex length varies with increasing Reynolds number. For $Re = 100$ in the fig. (11a), the vortex length of the was seen to be around 0.005m from the inlet. Subsequently, the maximum length of these regions for $Re = 1200, 1800$ and 2400 was $0.025m$, $0.035m$ and $0.05m$ (see fig. 11b, 11c and 11d respectively). The increase in the length of the vortex signifies that the suction pressure also increases with the increase in the velocity of the jet. Figure 12a shows the power spectrum of pressure fluctuations at the centre of the jet. Contours of cross-gradient components of velocity was plotted at the cross section of the channel for Re=1200 (see Fig.12b). This demonstrates the presence of secondary flow, especially dominant at the central region of the channel's cross section.

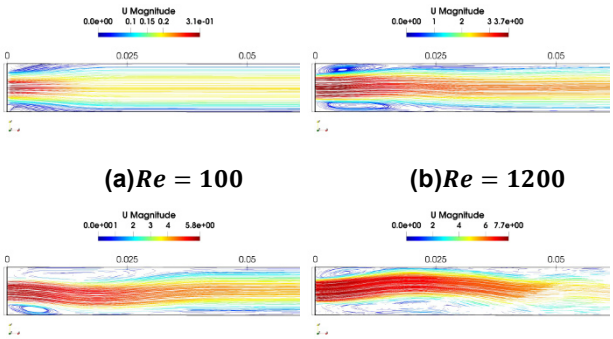

(a)$Re = 100$ (b)$Re = 1200$

(c)$Re = 1800$ (d)$Re = 2400$

Figure 11: Streamlines showing vortex length at fully developed condition ($x = 1.4m$ and $t = 4s$)

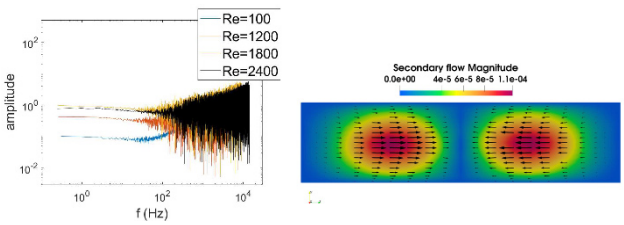

(a) (b)

Figure 12: (a) Power Spectrum of pressure fluctuation for different Reynolds number (b) Cross-gradient velocity vector plot of $Re = 1200$ at fully developed condition ($x = 1.4m$ and $t = 4s$)

4.4 Jet Fluctuations

The jet itself starts fluctuating with increase in the Reynolds number. Figure 13 shows the unsteady streamlines of the confined jet.

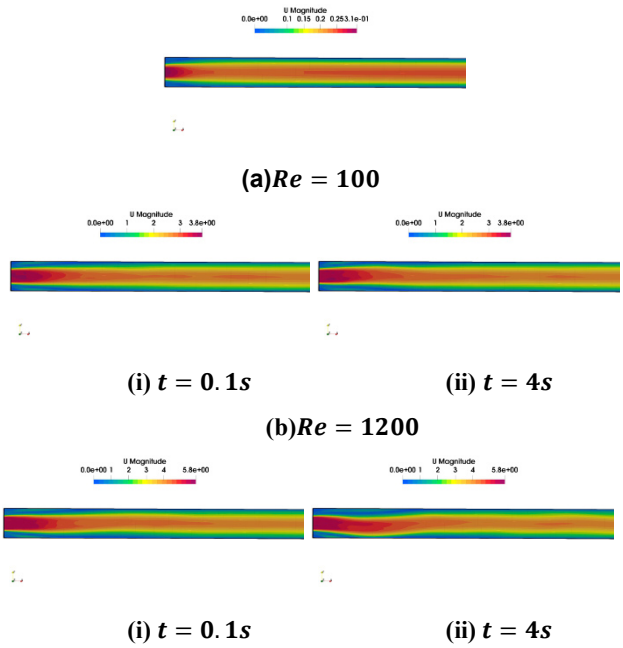

(a)$Re = 100$

(i) $t = 0.1s$ (ii) $t = 4s$

(b)$Re = 1200$

(i) $t = 0.1s$ (ii) $t = 4s$

(c)$Re = 1800$

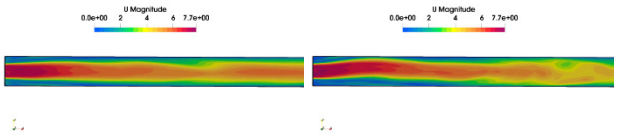

(i) $t = 0.1s$ **(ii) $t = 4s$**

(d)$Re = 2400$

Figure 13: Jet fluctuations with time

CONCLUSIONS

Simulations were carried out to investigate the flow behaviour of a planar jet in a confined channel with aspect ratio 0.25. Turbulence was modelled using LES as implemented in the opensource software OpenFoam. Simulations were performed for a wide range of Reynolds numbers between 100 and 2400. The fluid statistics were investigated in terms of the fluctuating velocity correlations and the Reynolds stress terms. In addition, the "Q" criterion was also determined. Fully developed velocity profile was compared against the analytical expression. The deviation from the analytical expression suggests a transitional flow in the channel at a Reynolds number lower than 1200. More simulations were performed and identified the transition at $Re \approx 500$ for the planar jet opening in a confined rectangular channel.

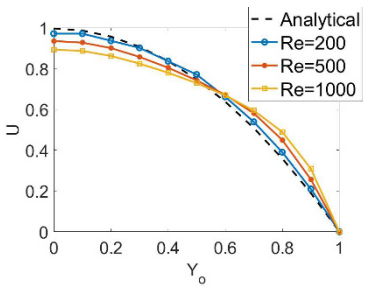

Figure 14: Comparison of the analytical velocity profiles to identify transition Re.

ACKNOWLEDGEMENTS

The authors would like to thank the supercomputing facility at Kathmandu University for providing access to its High Performance Computing facilities. The authors also thank Head, CC and Prof. Partha S Goswami for access to the supercomputing facility of IIT Bombay and cluster facility of Chemical Engineering, IIT Bombay. The first author thanks FOSSEE at IIT Bombay for the internship and Mr. Divyesh Variya for helping out in every problem.

NOMENCLATURE

A	Aspect ratio	--
t	Time	[s]
Δ	Height of the cell	[m]
P	Pressure	[kg/m-s^2]
Re	Reynolds number	--
u	Instantaneous velocity	[m-s^{-1}]
u'	Fluctuating velocity	[m-s^{-1}]
u_m	Mean velocity	[m-s^{-1}]
ν	Kinematic viscosity	[m^2-s^{-1}]
η	Kolmogorov's length scale	[m]

REFERENCES

[1] Trushar B. Gohil, Arun K. Saha, and K. Muralidhar, "Numerical study of instability mechanisms in a circular jet at low Reynolds numbers," *Computers and Fluids,* pp. 1-18, 2012.

[2] P. O'neill, J. Soria, and D. Honnery, "The stability of low Reynolds number round jets," *Experiments in Fluids,* vol. 36, pp. 473-483, 2004.

[3] Myoungkyu Lee and Robert D. Moser, "Direct numerical simulation of turbulent channel flow up to Re=5200," *Journal of Fluid Mechanics,* vol. 774, p. 395–415, 2015.

[4] Trushar B. Gohil, Arun K. Saha, and K. Muralidhar, "Direct numerical simulation of forced circular jets: Effect of varicose perturbation," *International Journal of Heat and Fluid Flow,* vol. 44, pp. 524-541, 2013.

[5] J. Cohen and I. Wygnanski, "The evolution of instabilities in the axisymmetric jet. Part 1. The linear growth of disturbances near the nozzle," *Journal of Fluid Mechanics,* vol. 176, p. 191–219, 1987.

[6] S. Gomé and S. L. Tuckerman, "Statistical transition to turbulence in plane channel flow," *Phys. Rev. Fluids,* 2020.

[7] R. W. Hanks and H. C. Ruo, "Laminar-Turbulent Transition in Ducts of Rectangular Cross Section," *Industrial \& Engineering Chemistry Fundamentals,* vol. 5, pp. 558-561, 1966.

[8] V. Theofilis, P. Duck, and J. Owen, "Viscous linear stability analysis of rectangular duct and cavity flows," *Journal of Fluid Mechanics,* vol. 505, 2004.

[9] Kim Lien, Jason Monty, Michelle Chong, and Andrew Ooi, "The Entrance Length for Fully Developed Turbulent Channel Flow," 2004.

[10] Raul Payri, J. Javier L´opez, Pedro Mart´ı-Aldarav´ı, and Jhoan S. Giraldo, "Effect of turbulent model closure and type of inlet boundary condition on a Large Eddy Simulation of a non-reacting jet with co-flow stream," *International Journal of Heat and Fluid Flow,* vol. 61, pp. 545-552, 2016.

[11] M. Klein, A. Sadiki, and J. Janicka, "Investigation of the influence of the Reynolds number on a plane jet using direct numerical simulation," *International Journal of Heat and Fluid Flow,* vol. 24, pp. 785-794, 2003.